Journal of Physics D: Applied Physics

PAPER • OPEN ACCESS

Characterization of $Cu(In,Ga)(Te,S)_2$ thin films grown on stainless steel foil substrates

To cite this article: Abdullah Karaca *et al* 2023 *J. Phys. D: Appl. Phys.* **56** 195302

View the article online for updates and enhancements.

You may also like

- A Diffusion Barrier for Flexible Thin Film Photovoltaics
Lian Guo, Maurice Mason, Marinus Hopstaken et al.

- Metal Capping Layer Effects on Electromigration Failure Phenomena of Plasma Etched Copper Lines
Jia Quan Su, Mingqian Li and Yue Kuo

- The effect of passivation-layer process to amorphous InGaZnO thin-film transistors using back-channel etch method
Yingtao Xie, Kunlin Cai, Penglong Chen et al.

244th ECS Meeting

Gothenburg, Sweden • Oct 8 – 12, 2023

Early registration pricing ends September 11

Register and join us in advancing science!

Learn More & Register Now!

This content was downloaded from IP address 79.123.161.175 on 31/08/2023 at 08:13

OPEN ACCESS
IOP Publishing
Journal of Physics D: Applied Physics
J. Phys. D: Appl. Phys. 56 (2023) 195302 (13pp)
https://doi.org/10.1088/1361-6463/acc40e

Characterization of $Cu(In,Ga)(Te,S)_2$ thin films grown on stainless steel foil substrates

Abdullah Karaca[1,2], Bülent M Başol[3], M Ali Olgar[4], Temel Büyüklimanlı[5], Murat Tomakin[6], Tayfur Küçükömeroğlu[1] and Emin Bacaksız[1,*]

[1] Department of Physics, Karadeniz Technical University, Trabzon, Turkey
[2] Department of Physics, Yozgat Bozok University, Yozgat, Turkey
[3] Active Layer Parametrics, Scotts Valley, CA, United States of America
[4] Department of Physics, Niğde Ömer Halisdemir University, Niğde, Turkey
[5] Eurofins EAG Laboratories, Sunnyvale, CA, United States of America
[6] Department of Physics, Recep Tayyip Erdoğan University, Rize, Turkey

E-mail: eminb@ktu.edu.tr

Received 8 November 2022, revised 3 February 2023
Accepted for publication 14 March 2023
Published 31 March 2023

Abstract

In this study, $Cu(In,Ga)(Te,S)_2$ (CIGTS) thin films with [Ga]/([In] ± [Ga]) atomic ratios in the ranges of 0.22–0.28 and 0.50–0.67 were fabricated using a two-stage technique. During the first stage of the technique, in one set of samples, Cu, In and Ga layers were deposited by electrodeposition on a Mo coated stainless steel (SS) foil substrate forming a SS/Mo/Cu/In/Ga precursor structure. For another set of samples, a Te layer was also deposited by e-beam evaporation on the SS/Mo/Cu/In/Ga structure forming a SS/Mo/Cu/In/Ga/Te precursor structure. During the second stage, SS/Mo/Cu/In/Ga and SS/Mo/Cu/In/Ga/Te stacks were reacted using rapid thermal annealing (RTA) for 5 min at 600 °C with or without presence of S vapors to produce CIGTS series thin films. SS/Mo/Cu/In/Ga stack under S atmosphere yielded $CuInGaS_2$ with a Ga-In gradient across the thickness by RTA process. SS/Mo/Cu/In/Ga/Te stack reacted without S in the reaction atmosphere yielded the $CuInGaTe_2$ compound. When S was present, the same stack with top Te layer yielded only $CuInGaS_2$ compound. When, however, already formed $CuInGaTe_2$ compound layers were heated in S environment at 400 °C, some Te could be retained in the films in the form of elemental Te. Gallium and In grading in various reacted films were evaluated by x-ray diffraction, secondary-ion mass spectrometry and EDS. CIGTS films showed highly (112) preferred oriented chalcopyrite phase and with the increase of Ga content, shifts were observed in the XRD peak positions demonstrating Ga inclusion in the lattice. Gibbs free energy calculations were used to explain the preferred reaction of S with metallic constituents when both S and Te were present for reaction.

Keywords: CIGS, CIGTS, foil substrate, RTA, chalcopyrite thin film, two stage process

(Some figures may appear in colour only in the online journal)

[*] Author to whom any correspondence should be addressed.

Original content from this work may be used under the terms of the Creative Commons Attribution 4.0 licence. Any further distribution of this work must maintain attribution to the author(s) and the title of the work, journal citation and DOI.

 © 2023 The Author(s). Published by IOP Publishing Ltd

1. Introduction

The optical band gap energy range of the semiconductor materials used as absorber layers in terrestrial thin film solar cell structures is ideally around 1.4–1.5 eV [1]. The group I-III-VI_2 semiconductor compounds have optical band gaps close to this range making them attractive for potential solar cell applications. However, bandgap by itself is not adequate to offer high efficiency devices. It is also important to examine the electronic properties of these compounds and to determine the optimum fabrication conditions. The reported optical band gap values for $CuInSe_2$ (CISe) and $CuGaSe_2$ ternary compounds are around 1.04 and 1.7 eV, respectively [2]. The optical band gap of CISe can be increased up to about 1.15 eV while preserving good electronic properties, by alloying with gallium and forming Cu(In,Ga)Se_2 (CIGSe) compund with a [Ga]/([In $\pm$ Ga]) atomic ratio of $\sim$0.3 [3]. Above this ratio the electronic properties generally deteriorate. Another approach to change the properties of CISe is adding sulfur (S) into the lattice forming CuIn(S,Se)$_2$ (CISSe). It is also possible to include both Ga and S in the material forming Cu(In,Ga)(S,Se)$_2$ (CIGSSe). Tuttle *et al*, for example, obtained CIGSSe/CdS solar cell structures by adjusting both the [Ga]/([In] $\pm$ [Ga]) ratio and the [S]/([S $\pm$ Se]) ratio. They determined the requirements for Ga and S doping profiles into the CISe lattice to be able to obtain high solar cell efficiency [4]. Therefore, the efficiency of CISe-based thin-film solar cells can be increased to higher values with Ga and S co-alloying. In the thin film photovoltaic (PV) industry, the CIGSSe compound is a widely studied material due to its high conversion efficiency (23.35%) and usage of low amounts of raw materials ($\sim$1–2 μm thick absorber layers) [5].

One of the commonly used techniques to synthesize CIGSe or CIGSSe material is the two-stage process, which includes deposition of metallic precursor layers comprising Cu, In and Ga, followed by a sulfurization/selenization process. The deposition of the precursor films can be done by various techniques such as sputtering [6], evaporation [7, 8], electrodeposition [9, 10], spin coating [11], etc. Among these techniques, sputtering has been the most commercialized technique and electrodeposition attracted much attention since it does not require vacuum and has provided reasonably high cell efficiencies in roll-to-roll manufacturing [12].

One commonly observed phenomenon in CIGSe thin film processing by two stage technique is the formation of a compositional gradient through the thickness of the film. Among other researchers, Başol *et al* examined the Ga distribution in CIGSe/CdS solar cell structures formed by a two-stage method and determined that Ga element was not homogeneously dispersed through the thickness of the compound. It was observed that gallium was concentrated near the back molybdenum (Mo) contact, leaving mostly a CISe crust layer at the top. It was shown that such a distribution caused a decrease in cell efficiency due to low voltage [13]. Probst *et al*, with their TEM measurements, found that in Mo/CIGSe thin film structure, the grain size of the compound near the Mo back contact was small and the grains got larger near the surface [14]. Weinhardt *et al* carried out atomic force microscopy (AFM) and x-ray photoelectron spectroscopy (XPS) measurements on CIGSSe layers and found a similar behavior. They also determined that S and Ga were agglomerated close to the Mo contact [15]. Overall, inhomogeneous compositional distribution in CIGSe and CIGSSe type films formed by the two-stage techniques is a known phenomenon that often causes lower device efficiencies if such gradients are not carefully designed and controlled. Gallium pile-up near the Mo contact is usually explained by kinetics of Ga-Se reaction, which is slower than In-Se reaction. As a result, Cu, In and Se react faster forming a CISe top crust, leaving Ga-rich phases behind. There has been attempts to influence this situation by changing certain process parameters such as the temperature ramping rates and the composition of the films. One approach studied was adding tellurium (Te) into the material.

Although use of Te as a interlayer to improve the quality of the CISe or CIGSe films was previously reported [16, 17], the Te amount in those studies was extremely small. As an alternative to CIGSe or CIGSSe compounds, a CuInGa(Te,Se)$_2$ (CIGTSe) absorber layer was proposed by our group for potential solar cell applications. Early results suggested that Ga distribution through the Cu(In,Ga)Te_2 (CIGT) films was more uniform than the CIGSe films [18]. Gremenoka *et al* investigated the structural, optical and electrical properties of CIGT films obtained by laser evaporation method and noted that the lattice parameter decreased and the forbidden energy gap increased with increasing Ga content in the material [19]. Although, there are some reported studies of CIGTSe material, there are no studies reported about Cu(In,Ga)(Te,S)$_2$ (CIGTS) chalcopyrite material comprising both S and Te in the lattice. In the present study, the structural and optical properties of CIGTS layers fabricated through a two-stage process have been evaluated as a function of Ga and Te content of these layers.

2. Experimental

The metallic precursor films of the two-stage process were prepared by electrodeposition over Mo-coated stainless steel foils (SS). This process step formed a SS/Mo/Cu-In-Ga structure with $x = [Ga]/([Ga] + [In])$ ratios in the ranges of 0.22–0.28 and 0.50–0.67. The targeted [Cu]/([In $\pm$ Ga]) ratio was in the 0.8–0.9 range. Metallic films were electrodeposited in the order of Cu/In/Ga, which is the easiest stack to form taking into account the deposition potentials of Cu, In and Ga elements. It should be noted that these structures were stored in laboratory environment for over a year before getting used in this research.

The SS substrates coated with Mo/Cu-In-Ga layers were cut into smaller (1 cm $\times$ 1 cm) pieces. Some of these samples were then placed in an e-beam evaporator for Te deposition. Pellets produced from Te powder (5 N-pure) were used as the source material. The distance between the samples and source was about 40 mm. The substrate was not intentionally heated during the Te deposition step and the coating was grown under a chamber pressure of 2×10^{-6} Torr. The thicknesses of Cu, In

Table 1. The thickness values of Cu, In, Ga and Te films and amount of sulfur (S).

Samples	Cu (nm)	In (nm)	Ga (nm)	Te (nm)	S (mg)
$CuIn_{0.7}Ga_{0.3}(Te,S)_2$	160	270	90	1125	30
$CuIn_{0.5}Ga_{0.5}(Te,S)_2$	171	194	150	1125	30

and Ga layers were determined by counting the charge passed through the stainless-steel substrate and the thickness of the Te layers was monitored using a crystal thickness monitor during e-beam evaporation. The film thicknesses of all layers are listed in table 1. It should be noted that, based on these thickness values one can calculate that the reacted compound layers would have an average thickness of about 1.5 μm.

For telluride formation, the stacks were reacted through a RTA process. For this process, samples were placed in a graphite box with a cover and internal dimensions of 50 mm × 20 mm × 12 mm. The box was placed in the vacuum tight quartz tube of the RTA system. Annealing was performed at 600 °C and under (5%) H_2 + (95%) Ar gas atmosphere for 5 min. To obtain films comprising S, Mo/Cu-In-Ga or Mo/Cu-In-Ga/Te stacks were sulphurized at 600 °C for 5 min under a sulfur atmosphere using 30 mg high purity sulfur powder as the source material. In other experiments, for the formation of $CuIn_{0.7}Ga_{0.3}(Te,S)_2$ and $CuIn_{0.5}Ga_{0.5}(Te,S)_2$ thin films, first telluride films (CIGT) were produced by using the RTA process without the S source, and then the CIGT samples that were formed this way were sulphurized at 400 °C–600 °C for 3 min in presence of S in the graphite box. It should be noted that an early study of $CuIn(S,Te)_2$ quaternary compound formation by standard melting and annealing technique showed that the chalcopyrite phase was formed for temperatures up to 650 °C. Above this temperature, phase transition was observed. Therefore, we selected the highest reaction temperature to be 600 °C [20].

The structural properties of the unreacted and reacted samples were characterized by x-ray diffraction (XRD). Raman spectroscopy measurements were carried out on the reacted samples. The chemical composition of the films was determined by energy dispersive x-ray (EDX) spectroscopy measurements. The surface and cross-sectional morphologies of the films were examined via scanning electron microscopy (SEM). Secondary-ion mass spectrometry (SIMS) was used to analyze the composition of the films through their thickness. Room temperature photoluminescence (PL) measurements were carried out. Temperature dependent Gibbs energy values were calculated to explain some of the findings. It should be noted that for the XRD measurements, incident angles of 0.3°, 0.5° and 5° were used. Considering the fact that the x-ray penetration depths at these angles are expected to be about 50 nm, 130 nm and 1000 nm, data at 0.3° and 0.5° grazing angles would probe the near-surface region, while the 5° data would represent the bulk properties of the layers [7]. Since the incoming angle for EDX measurements was also large, EDX data also represent bulk properties.

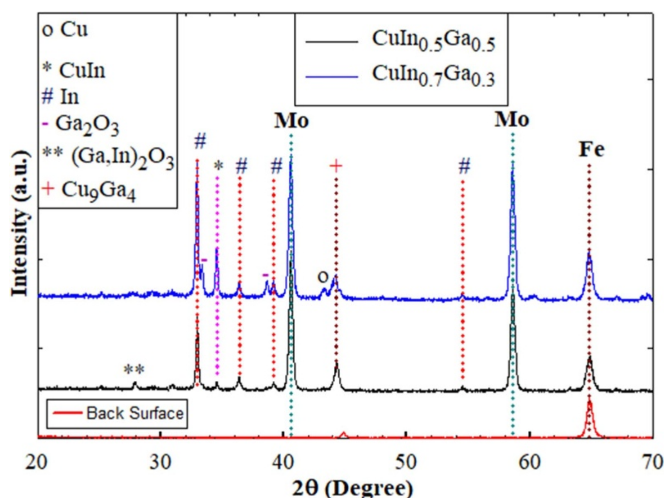

Figure 1. XRD pattern of $CuIn_{0.7}Ga_{0.3}$ and $CuIn_{0.5}Ga_{0.5}$ precursor films.

3. Results and discussion

The XRD patterns for the SS/Mo/Cu-In-Ga metallic precursor layers, formed during the first stage of the two-stage process, with two different Ga ratios are given in figure 1. As can be seen from this data the Cu-In-Ga precursors prepared with two different Ga ratios shared similar XRD patterns. As can be seen from this data the Cu-In-Ga precursors prepared with two different Ga ratios shared similar XRD patterns except that peaks corresponding to the Ga-oxide phases are more prominent for the 30% Ga containing film. It should be noted that these precursors were prepared using room-temperature electrolytes and they were not heat treated. However, they stayed in laboratory environment for over a year. As can be seen, despite the fact that there was no high temperature heat treatment, phases such as $(Ga,In)_2O_3$ (JPDS# 00-014-0564), Ga_2O_3 (JPDS# 00-006-0509), $CuIn_2$ (JPDS# 00-041-0255) and Cu_9Ga_4 (JPDS# 00-002-1253) were observed in the XRD patterns. In addition, elemental Cu (JPDS# 00-004-0836) and In (JPDS# 00-006-0416) peaks are also present. Mo (JPDS# 01-089-4896) and Fe ((JPDS# 00-087-0721) peaks are due to the underlying layers. The reasons why the lower Ga containing film shows more prominent Ga_2O_3 peaks and elemental Cu are not clear but it is possible that the thicker Ga film coated over the 50%Ga containing precursor may have formed a more continuous thin protective surface oxide, which does not show up in the XRD data. Such a thin surface oxide layer may prevent further oxidation of the underlying bulk of the film. With thinner Ga, the film may have larger surface area because of discontinuities and resulting roughness. Also the Ga-rich precursor may consume more of the Cu forming a compound and reducing the elemental Cu content of the film.

The XRD diffraction patterns of the reacted $CuIn_{0.7}Ga_{0.3}S_2$ films, formed after reaction during the second stage of the two-stage process, measured at different incident angles are given in figure 2. As seen in the figure, the characteristic peaks of

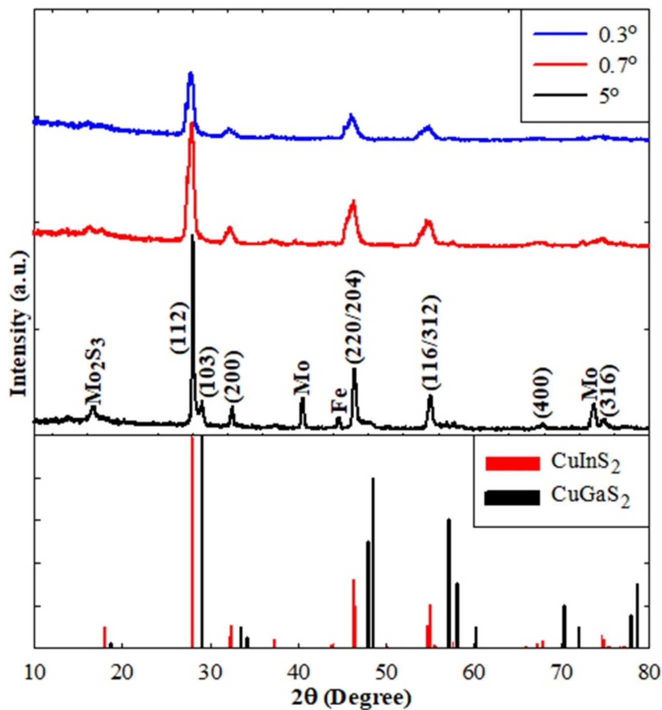

Figure 2. XRD patterns of $CuIn_{0.7}Ga_{0.3}S$ thin film taken by different incident angles.

(112), (200), (220/204) and (116/312) diffraction planes at approximate positions of $2\theta = 28.08°$, 32.58°, 46.72° and 55.16° were observed from XRD measurements performed at 0.3° incident angle. It is also seen that the dominant (112) and (220/204) peaks are split into two. One of these peaks is placed close to the expected peak position for $CuInS_2$ phase, the second peak is shifted towards larger angles suggesting Ga inclusion. With the increase of the incident angle from 0.3° to 0.7°, a similar diffraction pattern was obtained. However, it was observed that the peak positions were shifted slightly to higher angles, again in line with more Ga inclusion. With an increase of the incident angle to 5°, additional phases identified as Mo_2S_3 (JPDS#00-040-0972) at 16.71°, Fe at 44.72° (JPDS#01-085-1440), and Mo (JPDS#00-042-1120) at 40.46° and 73.68° were observed. Data collected at glazing incident angles of 0.3° and 0.7° represent the phase content of the near surface region of the film and it shows the presence of more In-rich phases. As the angle of incidence is increased to 5°, one expects to collect more information about phases close to the substrate. These results suggest that $CuIn_{0.7}Ga_{0.3}S_2$ formed by our two-stage approach resulted in a gradation of Ga within the film, the back of the film being more Ga-rich. Pure $CuInS_2$ (PDF#00-015-0681) and $CuGaS_2$ (PDF#03-065-2730) phase peak positions are also shown in figure 2 and they support the arguments above.

For S and Te containing film formation, two different approaches were investigated. In one approach Mo/Cu-In-Ga/Te stacks were sulphurized at 600 °C for 5 min under S atmosphere. In this case it was observed that no Te inclusion was achieved into the compound. Only CIGS phase was

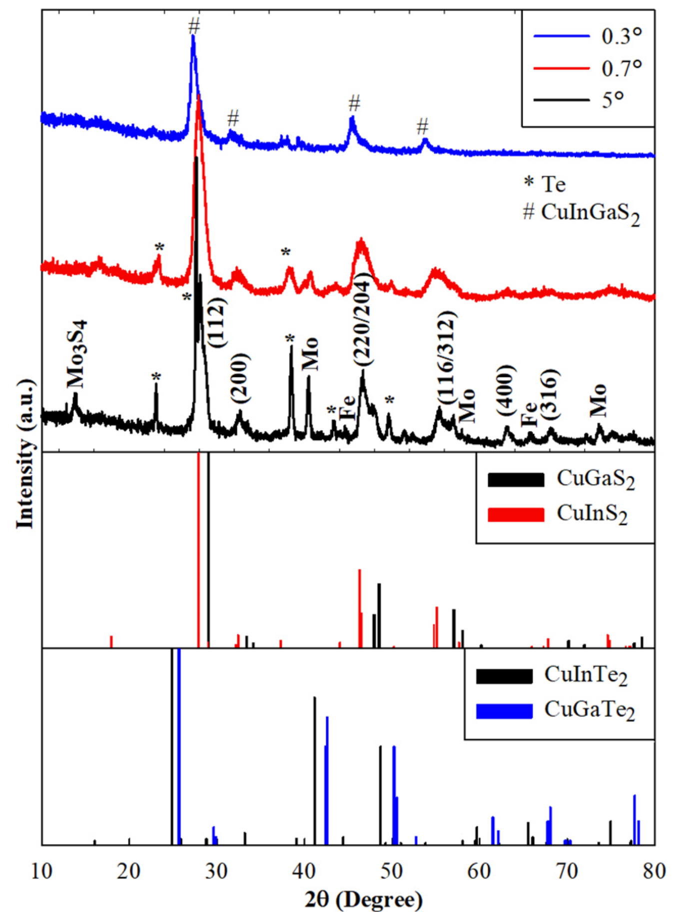

Figure 3. XRD patterns of $CuIn_{0.7}Ga_{0.3}(Te,S)_2$ sample taken by different incident angles.

formed. Therefore, another approach was employed, where first a CIGT layer was formed by reacting the Mo/Cu-In-Ga/Te stack at 600 °C for 5 min, and then the resulting compound was reacted with S at temperatures ranging from 600 °C to 400 °C. High sulfurization temperatures yielded again only CIGS layers, demonstrating that during sulfurization there was an exchange reaction causing complete replacement of Te in the compound with S. Reducing the reaction temperature to 400 °C and the reaction time to 3 min, we have seen some signature of Te in the films. Therefore, all data presented below regarding CIGTS layers are obtained using this second approach and the lower reaction temperature. It should be noted that samples processed to obtain CIGTS in this research are labeled as CIGTS, irrespective of their actual composition after the reaction step.

The XRD diffraction patterns of the $CuIn_{0.7}Ga_{0.3}(Te,S)_2$ samples taken at different incident angles are given in figure 3. The expected peak positions for $CuInTe_2$ (JPDS#00-034-1498) and $CuGaTe_2$ (JPDS#01-079-2331) phases are also shown in this figure. As can be seen from this data the XRD peaks observed are located at positions that are associated more with S-containing phases rather than Te-containing phases. The data at 0.3° belong to the (112) diffraction planes of the $CuInGaS_2$ phase with a [Ga]/([Ga ± In]) ratio of about

13%. With the increase of the incident angle from 0.3° to 0.7°, extra peaks are found that belong to the metallic Te phase at around $2\theta = 23.1°, 27.58°, 38.40°, 43.26°$ and 49.56° (JPDS#00-036-1452). This suggests that Te did not properly react and get included in the lattice of the compound. Solid phase reaction rate between Te and the other metallic elements in the stack may not be as fast or energetically favorable as reaction between the gaseous S and the metals. As a consequence, Cu, In and Ga in the precursor layers may have been grabbed by S, leaving behind elemental Te. It should be noted that the vapor pressure of Te at the reaction temperature is around 6×10^{-5} atmosphere, which is not enough for it to vaporize. The data taken at 5° displays the Mo and Fe phases originating from the back contact and the substrate, respectively. Formation of Mo_3S_4 (JP≠00-027-0319) phase is also observed in this data.

The incident angle dependent XRD patterns taken from $CuIn_{0.7}Ga_{0.3}Te_2$ films are presented in figure 4. As can be seen in the graph, just as in the $CuIn_{0.7}Ga_{0.3}S_2$ layers, most of the characteristic peaks of the chalcopyrite structure are split into two or more peaks. For example, peaks belonging to the dominant (112) reflection plane can be seen at 24.56° and 24.98° in the 0.3° data. As expected, the first peak (left one) belongs to In-rich $CuInGaTe_2$, while the second peak (right one) can be attributed to the Ga-rich $CuInGaTe_2$ phases. As discussed before, with reference to figure 2, Ga content in this structure is apparently also graded, Ga-rich material segregating towards the back of the film. This is obvious from the fact that the positions of the diffraction angles shifted towards higher angles with the increase of incidence angle. These results are consistent with the previously reported work on $CuInGa(Se,Te)_2$ semiconductor compounds [18].

The SEM and EDX measurement results of $CuIn_{0.7}Ga_{0.3}S_2$, $CuIn_{0.7}Ga_{0.3}(Te,S)_2$ and $CuIn_{0.7}Ga_{0.3}Te_2$ thin films are given in figure 5 and table 2. As can be seen in the figure, the surface morphologies of the samples are very different from each other. The feature size of the $CuIn_{0.7}Ga_{0.3}S_2$ sample is estimated to be in the range of 200–240 nm and the surface distribution is more homogeneous. The film structure is compact compared to the others. Inclusion of Te in the film changed the surface morphology completely. Specifically, surface roughness increased compared to the pure $CuIn_{0.7}Ga_{0.3}S_2$ film. In the $CuIn_{0.7}Ga_{0.3}Te_2$ sample, on the other hand, flake-like features are observed with sizes in the 0.5–1 μm range. Some porosity was also observed.

The results of EDX spectroscopy measurements are summarized in table 2. As can be seen in this table, all samples showed Cu-poor chemical composition regardless of the type of chalcogenide used in the reaction. This ratio is reasonably close to the one set during the electrodeposition of the precursors. The [Ga]/([Ga + In]) ratio is 0.22–0.28, again reasonably close to the targeted ratio of 0.3. Tellurium content in the CIGT layer is about 50%, as expected. For the CIGTS film, however, this percentage is only about 7.8%. Sulfur content is about 47.6%. XRD data for this film had shown presence of metallic Te. Therefore, the Te content given by EDX may be mostly due to this phase rather than due to the Te containing compound.

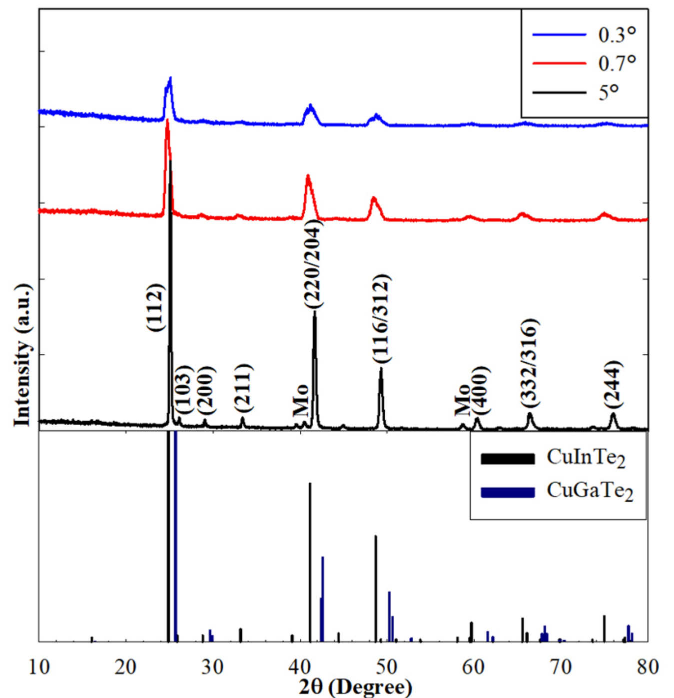

Figure 4. XRD patterns of $CuIn_{0.7}Ga_{0.3}Te_2$ sample taken by different incident angles.

To study the case of higher Ga-content samples, we repeated the above experiments for films with [Ga]/([Ga + In]) ratio of about 0.5. The XRD patterns of the $CuIn_{0.5}Ga_{0.5}S_2$ layers obtained after the reaction step are given in figure 6. As seen in this figure, the characteristic chalcopyrite peaks due to the (112), (220/204) and (116/312) diffraction planes are clearly split in the data obtained at low incident angles of 0.3° and 0.7°. This situation is more pronounced compared to the XRD patterns of the $CuIn_{0.7}Ga_{0.3}S_2$ film of figure 2. For example, the peak positions of the (112) plane was at 27.80°, 28.65°, 29.16° and the corresponding lattice distances were determined to be 3.21, 3.12 and 3.16 Å. This structure indicates formation of Ga-rich $CuInGaS_2$ compound close to the Mo back contact, while the surface has an In-rich crust. In addition to the increase in the intensity of all peaks with increasing incident angle, small peaks belonging to CuS (PDF#01-072-1071) phase can also be seen in the glancing angle data, suggesting near-surface formation of this phase, which has been observed before [21, 22]. EDAX measurement results for this sample are given in table 3 and it indicates a Cu-rich composition. Apparently, there was some In loss from this sample, possibly in the form of In_2S during the reaction step. This is the reason for CuS phase formation.

In figure 7, XRD patterns of $CuIn_{0.5}Ga_{0.5}(Te,S)_2$ samples are given. As in the case of figure 3, the diffraction peaks obtained at low angles show that there is a range of stoichiometries near the surface including In-rich CIGS. Tellurium does not seem to be alloyed with the compound. Data taken at 5° incident angle shows elemental Te peaks. It appears that both Ga-rich CIGS and Te reside deep in the film closer to the Mo contact. EDAX data in table 3 shows only about 2%

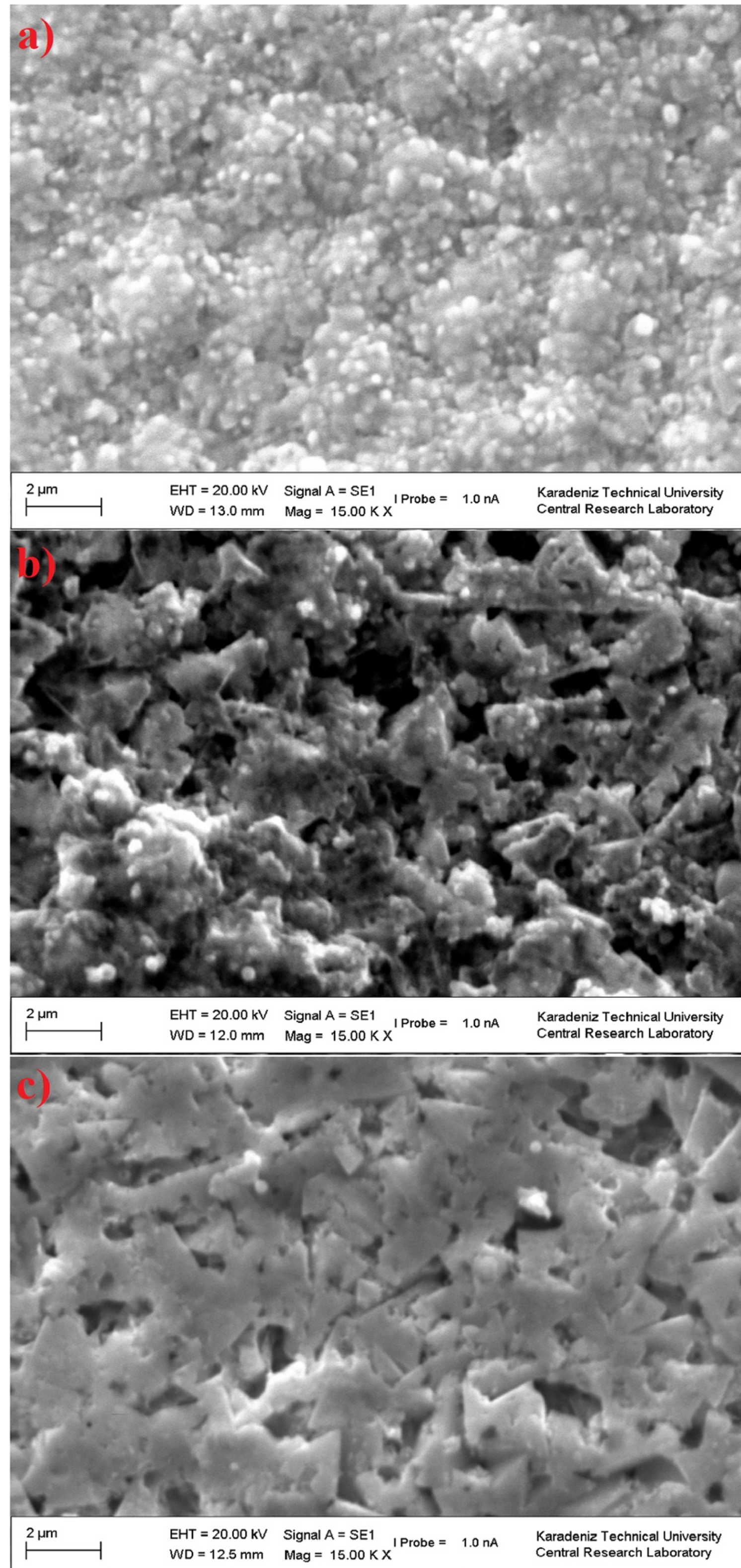

Figure 5. SEM surface image of (a) $CuIn_{0.7}Ga_{0.3}S_2$, (b) $CuIn_{0.7}Ga_{0.3}(Te,S)_2$, and (c) $CuIn_{0.7}Ga_{0.3}Te_2$ samples.

Table 2. Atomic percentage and some atomic ratios in $CuIn_{0.7}Ga_{0.3}S_2$, $CuIn_{0.7}Ga_{0.3}(Te,S)_2$, and $CuIn_{0.7}Ga_{0.3}Te_2$ samples.

Samples	Cu (%)	In (%)	Ga (%)	S (%)	Te (%)	Cu/(Ga + In)	Ga/(Ga + In)	S + Te/(Metal)
$CuIn_{0.7}Ga_{0.3}S_2$	22.1	17.5	5.0	55.4	—	0.98	0.22	1.24
$CuIn_{0.7}Ga_{0.3}(Te,S)_2$	20.9	17.1	6.8	47.6	7.8	0.87	0.28	1.24
$CuIn_{0.7}Ga_{0.3}Te_2$	21.9	20.5	7.9	—	49.7	0.77	0.28	0.99

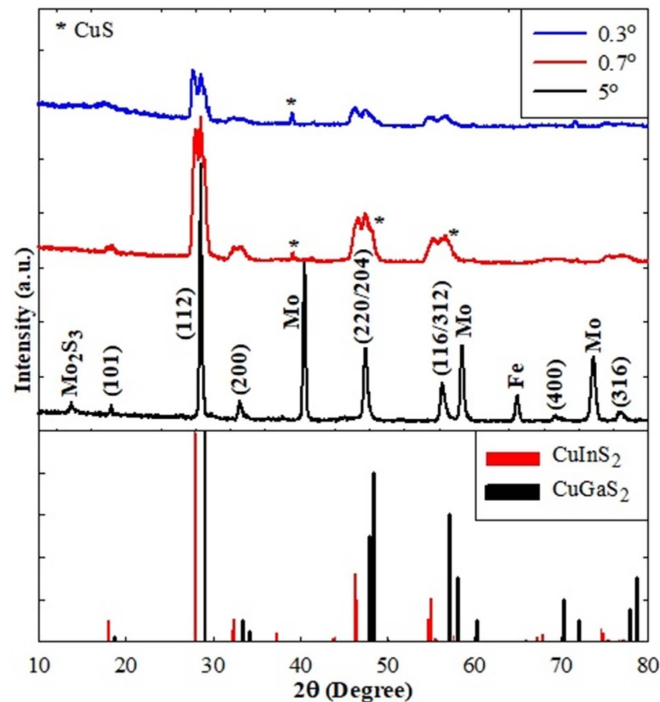

Figure 6. XRD patterns of $CuIn_{0.5}Ga_{0.5}S_2$ thin film taken by different incident angles.

Table 3. Atomic percentage and some atomic ratios in $CuIn_{0.5}Ga_{0.5}S_2$, $CuIn_{0.5}Ga_{0.5}(Te,S)_2$, and $CuIn_{0.5}Ga_{0.5}Te_2$ samples.

Samples	Cu (%)	In (%)	Ga (%)	S (%)	Te (%)	Cu/(Ga + In)	Ga/(Ga + In)	S + Te/(Metal)
$CuIn_{0.5}Ga_{0.5}S_2$	26.9	7.8	15.9	49.4	—	1.14	0.67	0.98
$CuIn_{0.5}Ga_{0.5}(Te,S)_2$	23.0	10.6	16.2	48.0	2.1	0.86	0.60	1.00
$CuIn_{0.5}Ga_{0.5}Te_2$	21.6	16.0	16.0	—	46.3	0.68	0.5	0.86

Te in the material. Clearly, reaction of S with the metallic precursor was more aggressive in this case also, as supported by the XRD data.

It should be noted that Landry *et al* attempted to obtain $CuInTe_{1-x}S_x$ compound in stoichiometric ratio using a mixture of CIT and CIS in a sealed tube. The mixture was heated by microwave and the resulting material was tested by XRD. It was found that after the reaction step CIS and CIT phases were still present but an additional $CuInS_{0.3}Te_{1.7}$ phase was detected. These researchers concluded that the solubility limit of S in this type of chalcopyrite crystal is around 0.3 [21, 22]. There are many differences between their approach and ours. First of all, they were reacting two compounds. Although the reaction temperature was not cited, it probably was very high. Most importantly, their reaction was carried out in a sealed ampule whereas our graphite box represents a leaky system since the cap is not vacuum tight sealed. Therefore, when we attempted reaction at 600 °C, Te was lost without any chance to react. At the low temperature of 400 °C, Te stayed but it was mostly in the form of the element since the reaction temperature was not high enough. These results demonstrate the difficulty of forming CIGTS compound layers using two stage processing in an unsealed reactor.

In figure 8, the XRD patterns of $CuIn_{0.5}Ga_{0.5}Te_2$ thin films are given. It was observed that all characteristic peaks were split into at least two components at small incident angles of 0.3° and 0.7°. In the same manner as in the XRD patterns of $CuIn_{0.7}Ga_{0.3}Te_2$ of figure 4, In-rich peaks were observed close to surface, and Ga-rich peaks were observed close to the substrate as can be seen from the data taken at 5° incident angle. The gradual shift of the peaks towards larger angles with the increase in the angle of incidence supports this interpretation.

Figure 9 shows the SEM surface and cross-sectional images taken from the $CuIn_{0.5}Ga_{0.5}S_2$, $CuIn_{0.5}Ga_{0.5}(Te,S)_2$

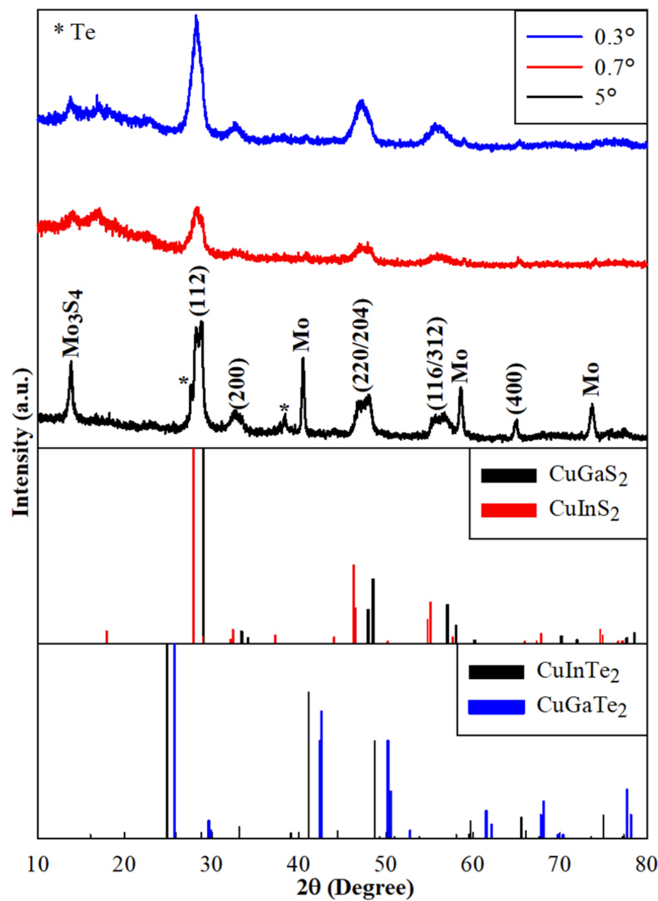

Figure 7. XRD patterns of $CuIn_{0.5}Ga_{0.5}(Te,S)_2$ thin film taken by different incident angles.

and $CuIn_{0.5}Ga_{0.5}Te_2$ samples. As seen in this figure, all samples revealed dense polycrystalline microstructures. While surface the of the $CuIn_{0.5}Ga_{0.5}S_2$ thin film displayed small grains, the Te-doping contributed to coalescence of the small grains and formation of larger grains. The surface of the $CuIn_{0.5}Ga_{0.5}Te_2$ film also showed formation of larger faceted grains compared to the $CuIn_{0.5}Ga_{0.5}S_2$ film. The cross-sectional images suggest dense film structure with thickness in the order of 1.5–2 μm. The $CuIn_{0.5}Ga_{0.5}S_2$ sample has a rougher surface structure and the light colored crystallites are associated with the CuS phase as detected by energy dispersive x-ray spectroscopy (EDS) and XRD.

The SIMS measurements were carried out on the $CuIn_{0.5}Ga_{0.5}S_2$ and $CuIn_{0.5}Ga_{0.5}Te_2$, which represent the properly reacted compound layers.

As can be seen from figure 10(a), the compositional distributions of the elements in the $CuIn_{0.5}Ga_{0.5}S_2$ sample showed variation through the thickness of the film. While the compositional distribution of Cu and S element showed rather uniform distribution, the In and Ga concentration showed gradient structure. The surface of the sample displayed In-rich and the back region displayed Ga-rich composition. This is consistent with the XRD data. Reason for Ga gradation is the difference between Cu-In-S and Cu-Ga-S reactions, the former being much faster. Therefore, during reaction a crust of In-rich compound forms leaving behind the Ga-rich phases.

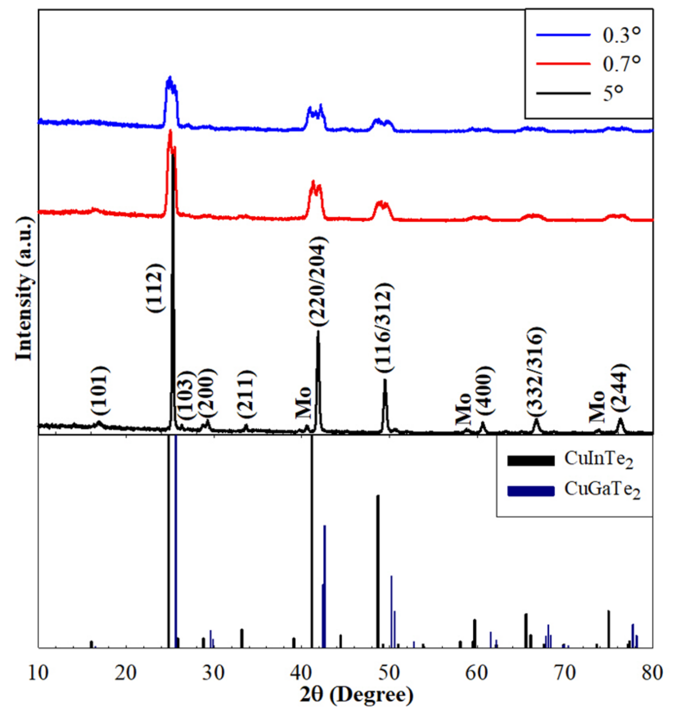

Figure 8. XRD patterns of $CuIn_{0.5}Ga_{0.5}Te_2$ thin film taken by different incident angles.

The reason why Mo signal is recorded as early as 0.5 μm into the film is the fact that these layers have rough surface morphology and the thickness may be varying between 0.5–2 μm. The SIMS plot taken from the $CuIn_{0.5}Ga_{0.5}Te_2$ film is given in figure 10(b). As can be seen from this data, distribution of In and Ga through the telluride film is more uniform compared to the sulfide film.

The chemical compositions of the $CuIn_{0.5}Ga_{0.5}S_2$, $CuIn_{0.5}Ga_{0.5}(Te,S)_2$, and $CuIn_{0.5}Ga_{0.5}Te_2$ samples are summarized in table 3. As shown in this table, the $CuIn_{0.5}Ga_{0.5}S_2$ sample has Cu-rich composition and the other samples contain less Cu. The $CuIn_{0.5}Ga_{0.5}(Te,S)_2$ sample showed less Te compared to the $CuIn_{0.7}Ga_{0.3}S_2$ sample. The Te might not be incorporated in structure of this sample. It was concluded that regardless of the Ga atomic ratio Te did not effectively react and got included into the $CuIn_{0.5}Ga_{0.5}S_2$ lattice. To interpret these interesting and somewhat unexpected results, the Gibbs energy calculations were carried out using the HSC Chemistry 7.14 program. The Gibbs energy is defined by the following equation;

$$G = G_0 + RT\ln Q \tag{1}$$

where Q is the reaction rate, T is the temperature, and R is the ideal gas constant. The curves showing the variation of Gibbs energy with temperature, calculated for $CuIn_{0.5}Ga_{0.5}(Te,S)_2$, are given in figure 11.

The possible reaction pathways for these compounds may be given by the following equations;

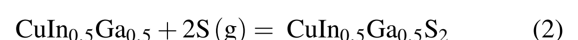

$$CuIn_{0.5}Ga_{0.5} + 2S\,(g) = CuIn_{0.5}Ga_{0.5}S_2 \tag{2}$$

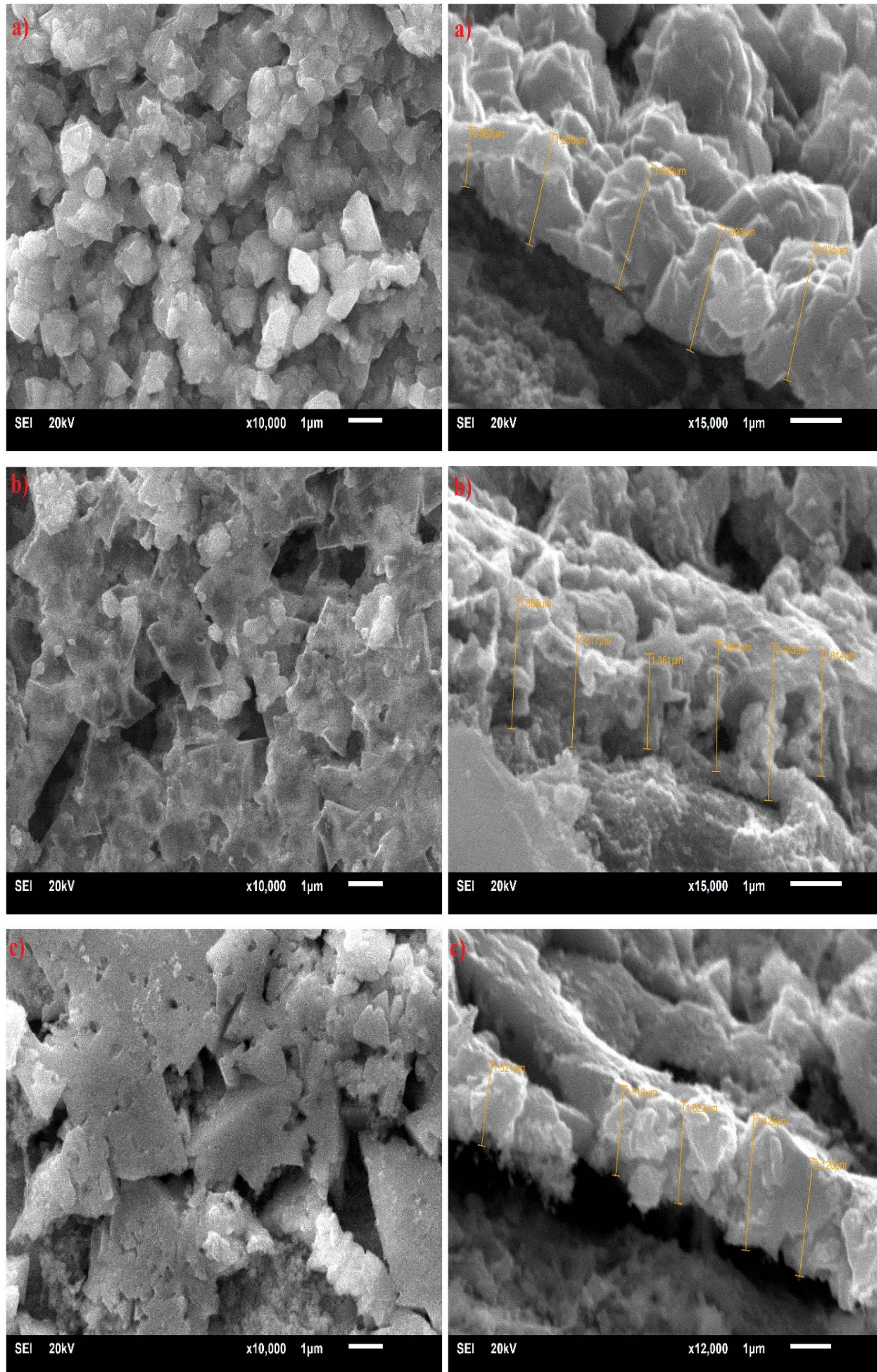

Figure 9. SEM surface and cross-sectional image of (a) $CuIn_{0.5}Ga_{0.5}S_2$ (b) $CuIn_{0.5}Ga_{0.5}(Te,S)_2$, and (c) $CuIn_{0.5}Ga_{0.5}Te_2$ samples.

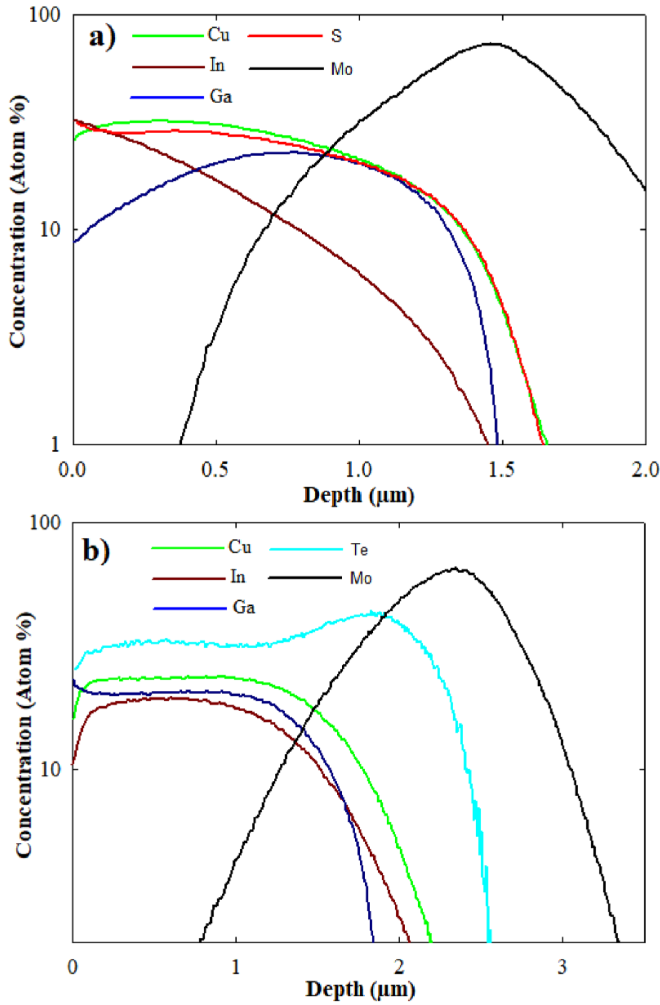

Figure 10. SIMS measurement of (a) $CuIn_{0.5}Ga_{0.5}S_2$, (b) $CuIn_{0.5}Ga_{0.5}Te_2$ samples.

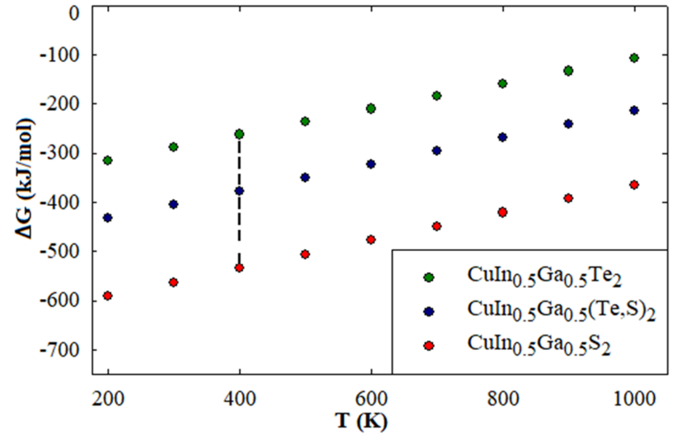

Figure 11. Gibbs energy calculation of $CuIn_{0.5}Ga_{0.5}(Te,S)_2$ series samples.

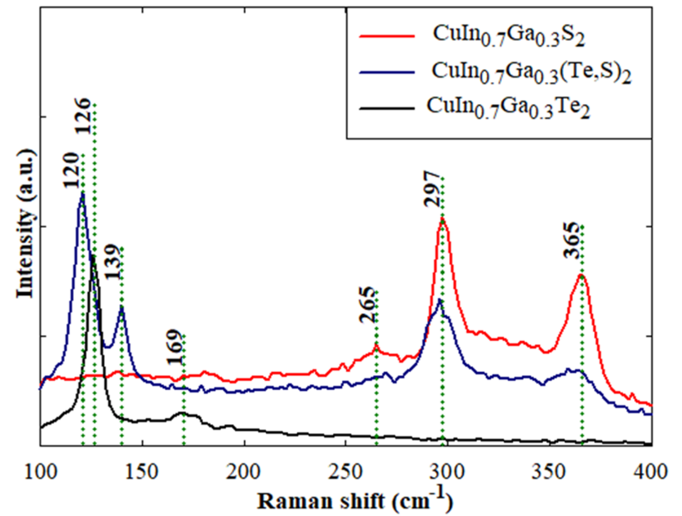

Figure 12. Raman spectra of $CuIn_{0.7}Ga_{0.3}S_2$, $CuIn_{0.7}Ga_{0.3}(Te,S)_2$, and $CuIn_{0.7}Ga_{0.3}Te_2$ samples.

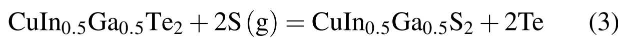

$$CuIn_{0.5}Ga_{0.5}Te_2 + 2S\,(g) = CuIn_{0.5}Ga_{0.5}S_2 + 2Te \quad (3)$$

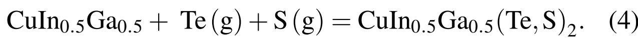

$$CuIn_{0.5}Ga_{0.5} + \,Te\,(g) + S\,(g) = CuIn_{0.5}Ga_{0.5}(Te,S)_2. \quad (4)$$

More negative Gibbs energy means more energetically favorable reaction, ignoring the possible kinetic effects. Data in figure 11 suggests that formation of CIGTS from reaction of Cu-In-Ga compounds with Te and S is less favorable than formation of CIGS. Therefore, in an environment where S and Te are present together, CIGS formation does not allow Te to be included in the lattice. This explains our results and the explanations provided earlier in this manuscript. It should be noted that Zhang *et al* recently reported results of an experiment where CdTe compound was reacted with S in vacuum under different temperature and pressure values. They observed that S completely exchanged with Te and CdTe was converted into CdS [23]. We have shown a similar phenomenon for reaction of CIGT compound with S.

It is known that the $CuInS_2$, $CuGaS_2$, $CuInTe_2$ and $CuGaTe_2$ semiconductor compounds crystallize in the chalcopyrite structure that have 24 vibration modes, 21 of which are optical and the others are acoustic. In these vibration modes ($1A_1 + 2A_2 + 3B_1 + 3B_2 + 6E$) all optical modes except A_2 are active, while B_2 and E are active only in the infrared region. Figure 12 presents the Raman spectra data obtained from the $CuIn_{0.7}Ga_{0.3}S_2$, $CuIn_{0.7}Ga_{0.3}(Te,S)_2$ and $CuIn_{0.7}Ga_{0.3}Te_2$ samples. As can be seen from this figure, the spectra are dominated by a peak located at around 297 cm^{-1} that is attributed to A_1 mode of the $CuInGaS_2$ compound. This peak is present for both CIGS and CIGTS samples. Other peaks (265 cm^{-1} and 365 cm^{-1}) of the same phase are also marked in the figure. According to the literature the A_1 mode for $CuInS_2$ and $CuGaS_2$ phases are expected to be at around 290 cm^{-1} and 310 cm^{-1}, respectively, In the $CuIn_{0.7}Ga_{0.3}S_2$ film it is observed that the A_1 mode is seen at a location in between these values, as expected, as a result of the gradual replacement of In atoms with Ga atoms. In addition, as a result of growing the $CuInGaS_2$ compound as Cu-rich and Cu-poor, shifts may occur in the peak positions. The origin of the peak around 265 cm^{-1} with weak peak intensity may be controversial. In

the literature, this peak may be attributed to the CuS phase or E(TO) mode of the $CuGaS_2$ semiconductor compound. The peak observed at 365 cm^{-1} position can be ascribed to the B_2(LO) mode of $CuGaS_2$ [24–26]. Metallic Te peaks were observed in the XRD data of the $CuIn_{0.7}Ga_{0.3}(Te,S)_2$ sample. Therefore, the peaks observed at 120 and 139 cm^{-1} positions in the Raman spectrum of the CIGTS sample may belong to the Te phase. Because Te has high atomic number and large electronic polarizability, it can show strong Raman active phonon modes [27]. The Raman spectra showed typical bands corresponding to the D3 symmetry group of the Te lattice with one A_1 mode and one degenerate E mode. The strong bands at 120 cm^{-1} for Te crystal are assigned to the A_1 mode, described by the symmetric intrachain expansion and compression in the *ab* plane (basal plane). The weak band centered around 139 cm^{-1} for Te NWs is assigned to the E_2 mode mainly described by the asymmetric stretching along the *c*-axis [28]. Raman spectra of the $CuInGaTe_2$ film, displayed peaks at around 126 and 169 cm^{-1}. The first peak may belong to the A_1 mode of $CuInTe_2$, while the second peak may belong to the $\left[E_1^5\right]$ mode of $CuInTe_2$ or the [B_2-E] mode of CuGaTe2. In the literature, while the peak positioned at around 125 cm^{-1} may be attributed to A_1 mode of $CuInTe_2$, the peak located at around 136 cm^{-1} can be ascribed to A_1 mode of $CuGaTe_2$ [29, 30].

The Raman spectra of the $CuIn_{0.5}Ga_{0.5}S_2$, $CuIn_{0.5}Ga_{0.5}(Te,S)_2$ and $CuIn_{0.5}Ga_{0.5}Te_2$ thin films are given in figure 13. As can be seen, the spectrum of the $CuIn_{0.5}Ga_{0.5}S_2$ film is dominated by 298 and 365 cm^{-1} peaks, as observed in the $CuIn_{0.7}Ga_{0.3}S_2$ samples. The dominant peak at 297 cm^{-1} for the 30% Ga sample shifted to a higher frequency with the increase of the Ga doping. No significant change was observed in the position of the 365 cm^{-1} peak. It was observed that the spectra of the CIGTS sample were similar to the spectra of the $CuInGaS_2$, both in the positions of the peaks and no additional peaks were found. This is an expected situation due to the fact that the amount of Te is very small in the structure (see table 2). It was observed that the peak observed at 126 cm^{-1} in the $CuIn_{0.7}Ga_{0.3}Te_2$ sample shifted to 129 cm^{-1} in the $CuIn_{0.5}Ga_{0.5}Te_2$ film. The reason for this can be explained by the increase in the Ga content.

The room-temperature PL measurements of the $CuIn_{0.7}Ga_{0.3}S_2$, $CuIn_{0.7}Ga_{0.3}Te_2$, $CuIn_{0.5}Ga_{0.5}S_2$ and $CuIn_{0.5}Ga_{0.5}Te_2$ films are presented in figure 14. Since the PL spectra of the CIGTS samples exhibited almost the same spectrum as the CIGS films, this data is not shown. As seen in the figure 14, since the PL peak intensities of CIGT thin films were very low compared to the CIGS samples, regardless of the Ga ratio, the CIGT data was multiplied by a certain coefficient. Similar PL curves were obtained for both $CuIn_{0.7}Ga_{0.3}$ and $CuIn_{0.5}Ga_{0.5}$ samples regardless of the Ga-content. An intense peak at around 1.55 eV was observed in the $CuInGaS_2$ samples regardless of the [Ga]/([In ± Ga]) atomic ratio. In the literature, the peak observed at 1.35 eV in Cu-rich samples is attributed to Cu_{In} and V_{In} defects, while the peak observed at 1.62 eV is attributed to band-to-band transition. In

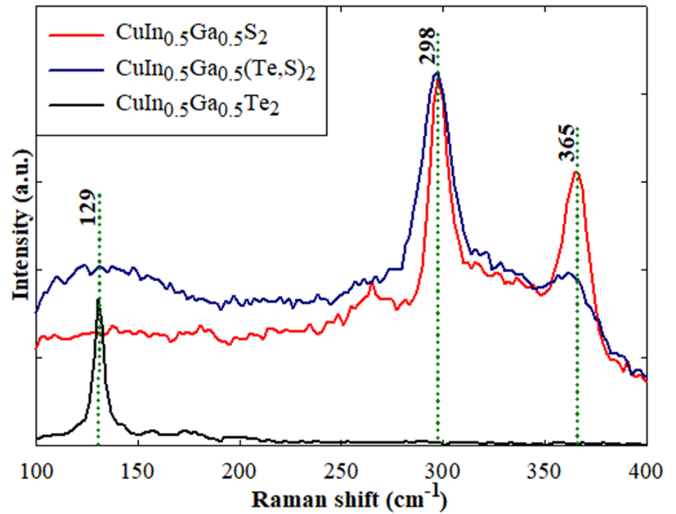

Figure 13. Raman spectra of $CuIn_{0.5}Ga_{0.5}S_2$, $CuIn_{0.5}Ga_{0.5}(Te,S)_2$, and $CuIn_{0.5}Ga_{0.5}Te_2$ samples.

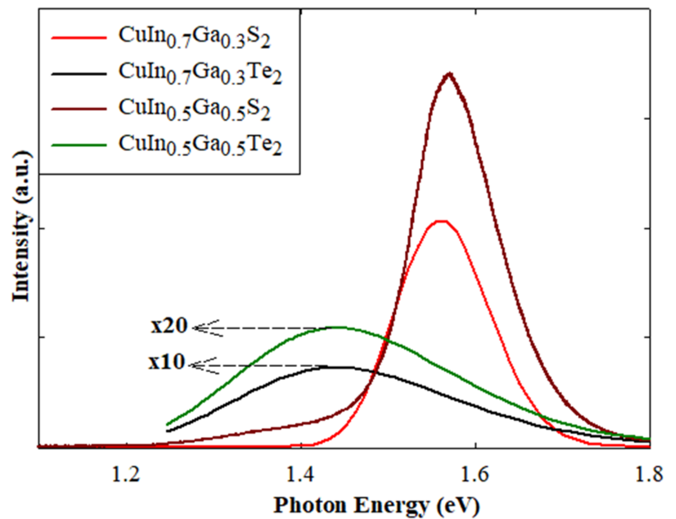

Figure 14. PL spectra of $CuIn_{0.7}Ga_{0.3}S_2$, $CuIn_{0.7}Ga_{0.3}Te_2$, $CuIn_{0.5}Ga_{0.5}S_2$ and $CuIn_{0.5}Ga_{0.5}T_2$ samples.

Cu-poor samples, the 1.62 eV peak may shift to lower energy values [31].

It is possible to come across very different interpretations in the literature regarding the band structure of the $CuInGaTe_2$ semiconductor compound. Yandjah *et al* recorded a band gap value of 0.87 eV and 1.2 eV from PL measurements for $CuIn_{0.5}Ga_{0.5}Te_2$ thin films [32]. In experiments only one peak was observed at around 1.42 eV, as seen in the figures. One probable reason why no other PL peaks are not observed may be related to the wavelength of the excitation source. In our PL measurements, the samples were excited at 633 nm/17.8 mW (He-Ne) laser source, while Krustok *et al* were excited using a 441 nm/40 mW (He-Cd) laser source [33]. In addition, the intensity of the signal in these measurements was very weak. Considering the fact that there may be contributions from

intrinsic defects and donor-acceptor pair recombination, we cannot conclusively say that the bandgap value is 1.42 eV. However, it is clear that the bandgap is smaller than the S containing compound, which is in line with the expectation.

4. Conclusions

$Cu(In,Ga)(Te,S)_2$ (CIGTS) with ([Ga]/([Ga + In]) ratios of 0.3 and 0.5 and various S and Te content were prepared on Mo coated SS foils using a two-stage technique. The technique involved electrodeposition of Cu/In/Ga stacks, evaporation of Te and reaction through RTA with or without S. SEM and XRD analysis showed that $Cu(In,Ga)(Te,S)_2$ thin films were well crystallized with compact and faceted grains and had strong (112) preferred orientation. Glancing angle XRD taken at 0.3° incident angle showed that in general In-rich phases were seen at the surface, while the Ga-rich phases were near the Mo contact. In films that were reacted simultaneously with Te and S at high temperature, no Te inclusion was observed. Some Te could be included in the CIGTS films if a CIGT layer was reacted with S at the low temperature of 400 °C. Gibbs free energy calculations showed reactions with S were more energetically favored.

Data availability statement

All data that support the findings of this study are included within the article (and any supplementary files).

Acknowledgments

Special thanks to Dr Gary Goodman of Eurofins-EAG Laboratories for the SIMS characterization of the samples.

CRediT authorship contribution statement

Abdullah Karaca: Writing—review & editing, Writing—original draft, Methodology, Investigation, Conceptualization. Bülent M. Başol: Writing—original draft, Methodology, Conceptualization. M. Ali Olgar: Methodology, Formal analysis. Temel Büyüklimanlı: Formal analysis. Murat Tomakin: Formal analysis. Tayfur Küçükömeroğlu: Methodology, Formal analysis. Emin Bacaksız: Writing—review & editing, Conceptualization.

ORCID iD

Emin Bacaksız https://orcid.org/0000-0002-0041-273X

References

[1] Boxwell M 2010 *Solar Electricity Handbook: A Simple, Practical Guide to Solar Energy-designing and Installing Photovoltaic Solar Electric Systems* (Birmingham: Greenstream publishing)
[2] Papadimitriou D, Esser N and Xue C 2005 *Phys. Status Solidi* b **242** 2633–43
[3] Platzer-Björkman C, Hultqvist A, Pettersson J and Törndahl T 2010 *Oxide-based Materials and Devices* vol 7603 (SPIE) pp 82–90
[4] Tuttle J, Sites J, Delahoy A, Shafarman W, Baso B, Fonash S, Gray J, Menner R, Phillips J and Rockett A 1995 *Prog. Photovolt., Res. Appl.* **3** 89–104
[5] Nakamura M, Yamaguchi K, Kimoto Y, Yasaki Y, Kato T and Sugimoto H 2019 *IEEE J. Photovolt.* **9** 1863–7
[6] Shi J, Li Z, Zhang D, Liu Q, Sun Z and Huang S 2011 *Prog. Photovolt., Res. Appl.* **19** 160–4
[7] Repins I, Contreras M A, Egaas B, DeHart C, Scharf J, Perkins C L, To B and Noufi R 2008 *Prog. Photovolt., Res. Appl.* **16** 235–9
[8] Qi T, Zhao C, Liu Y, Liu X, Zheng X, Ning D, Ma M, Feng Y, Chen M and Li W 2022 *Mater. Sci. Semicond. Process.* **149** 106879
[9] Aksu S, Wang J and Basol B M 2009 *Electrochem. Solid-State Lett.* **12** D33
[10] Tsai C-L, Huang K-M and Jeng M-J 2013 *Mater. Sci. Semicond. Process.* **16** 1599–602
[11] Al-Saidi S S, Ali O A and AL-Awadi S S 2021 *AIP Conf. Proc.* **2372** 080011
[12] Başol B, Pinarbasi M, Aksu S, Wang J, Matus Y, Johnson T, Han Y, Narasimhan M and Metin B 2008 *23th European Photovoltaic Solar Energy Conf.*
[13] Basol B, Kapur V, Norsworthy G, Halani A, Leidholm C and Roe R 1998 *Electrochem. Solid-State Lett.* **1** 252
[14] Probst V, Stetter W, Riedl W, Vogt H, Wendl M, Calwer H, Zweigart S, Ufert K-D, Freienstein B and Cerva H 2001 *Thin Solid Films* **387** 262–7
[15] Weinhardt L, Fuchs O, Peter A, Umbach E, Heske C, Reichardt J, Bär M, Lauermann I, Kötschau I and Grimm A 2006 *J. Chem. Phys.* **124** 074705
[16] Basol B M, Kapur V K and Matson R J 1991 *Conf. Record of the Twenty-Second IEEE Photovoltaic Specialists Conf.*
[17] Kim K, Han J and Shafarman W N 2013 *MRS Online Proc. Library (OPL)*
[18] Atasoy Y, Başol B M, Olğar M A, Tomakin M and Bacaksız E 2018 *Thin Solid Films* **649** 30–37
[19] Gremenoka V, Martinb R, Bodnara I, Yakushevb M, Schmitzc W, Bentec K, Martild I, Martinezd F, Zaretskayaa E and Victorova I 2001 *Thin Solid Films* **394** 24–29
[20] Grima P, Quintero M, Rincón C, Peres G and Woolley J C 1988 *Solid State Commun.* **67** 81–83
[21] Landry C C, Lockwood J and Barron A R 1995 *Chem. Mater.* **7** 699–706
[22] Olgar M A, Klaer J, Mainz R, Levcenco S, Just J, Bacaksiz E and Unold T 2016 *Thin Solid Films* **615** 402–8
[23] Zhang X, Liu D, Jiang W, Xu W, Deng P, Deng J and Yang B 2020 *J. Mater. Res. Technol.* **9** 6977–86
[24] Shukla S, Adeleye D, Sood M, Ehre F, Lomuscio A, Weiss T P, Siopa D, Melchiorre M and Siebentritt S 2021 *Phys. Rev. Mater.* **5** 055403
[25] Guijarro N, Prévot M S, Johnson M, Yu X, Bourée W S, Jeanbourquin X A, Bornoz P, Le Formal F and Sivula K 2016 *J. Phys. D: Appl. Phys.* **50** 044003
[26] Neisser A, Hengel I, Klenk R, Matthes T W, Alvarez-Garcıa J, Pérez-Rodrıguez A, Romano-Rodrıguez A and Lux-Steiner M-C 2001 *Sol. Energy Mater. Sol. Cells* **67** 97–104
[27] Luo Q, Tang G, Sun M, Qian G, Shi Z, Qian Q and Yang Z 2020 *Opt. Mater. Express* **10** 1072–82

[28] Silva R R, Mejia H A, Ribeiro S J, Shrestha L K, Ariga K, Oliveira O N, Camargo V R, Maia L J and Araújo C B 2017 *J. Braz. Chem. Soc.* **28** 58–67
[29] Rincón C, Wasim S, Marín G, Hernández E, Delgado J and Galibert J 2000 *J. Appl. Phys.* **88** 3439–44
[30] Kesari S, Salke N P and Rao R 2016 *AIP Conf. Proc.* **1731** 030012
[31] Kim S, Nagai T, Tampo H, Ishizuka S and Shibata H 2020 *Prog. Photovolt., Res. Appl.* **28** 816–22
[32] Yandjah L, Bechiri L, Benabdeslem M, Benslim N, Amara A, Portier X, Bououdina M and Ziani A 2018 *Chin. J. Phys.* **56** 904–10
[33] Krustok J, Grossberg M, Jagomägi A, Danilson M and Raudoja J 2007 *Thin Solid Films* **515** 6192–5